Partial drift volume due to a self-propelled swimmer

Nicholas G. Chisholm* and Aditya S. Khair†
Department of Chemical Engineering, Carnegie Mellon University, 5000 Forbes Avenue, Pittsburgh, Pennsylvania 15213, USA

(Received 5 September 2017; published 5 January 2018)

We assess the ability of a self-propelled swimmer to displace a volume of fluid that is large compared to its own volume via the mechanism of partial drift. The swimmer performs rectilinear locomotion in an incompressible, unbounded Newtonian fluid. The partial drift volume D is the volume of fluid enclosed between the initial and final profiles of an initially flat circular disk of marked fluid elements; the disk is initially aligned perpendicular to the direction of locomotion and subsequently distorted due to the passage of the swimmer, which travels a finite distance. To focus on the possibility of large-scale drift, we model the swimmer simply as a force dipole aligned with the swimming direction. At zero Reynolds number ($\mathrm{Re} = 0$), we demonstrate that D grows without limit as the radius of the marked fluid disk h is made large, indicating that a swimmer at $\mathrm{Re} = 0$ can generate a partial drift volume much larger than its own volume. Next, we consider a steady swimmer at small Re, which is modeled as the force-dipole solution to Oseen's equation. Here, we find that D no longer diverges with h, which is due to inertial screening of viscous forces, and is effectively proportional to the magnitude of the force dipole exerted by the swimmer. The validity of this result is extended to $\mathrm{Re} \geqslant O(1)$—the realm of intermediate-Re swimmers such as copepods—by taking advantage of the fact that, in this case, the flow is also described by Oseen's equations at distances much larger than the characteristic linear dimension of the swimmer. Next, we utilize an integral momentum balance to demonstrate that our analysis for a steady inertial swimmer also holds, in a time-averaged sense, for an unsteady swimmer that does not experience a net acceleration over a stroke cycle. Finally, we use experimental data to estimate D for a few real swimmers. Interestingly, we find that D depends heavily on the kinematics of swimming, and, in certain cases, D can be significantly greater than the volume of the swimmer at $\mathrm{Re} \geqslant O(1)$. Our work also highlights that D due to a self-propelled body is fundamentally different than that due to a body towed by an external force. In particular, predictions of D in the latter case cannot be utilized to estimate D for a self-propelled swimmer.

DOI: 10.1103/PhysRevFluids.3.014501

I. INTRODUCTION

When an object moves through a fluid, it displaces the surrounding fluid elements from their original positions. This phenomenon is referred to as *drift* [1]. Drift induced by swimming organisms is of particular interest because it is a mechanism by which these organisms can achieve biogenic mixing of the surrounding fluid. Quantifying biogenic mixing, or biomixing, is important because among the matter present in the fluid are nutrients and dissolved substances (e.g., oxygen, carbon

*Present address: Department of Chemical and Biological Engineering, University of Pennsylvania; nchishol@alumni.cmu.edu
†akhair@andrew.cmu.edu

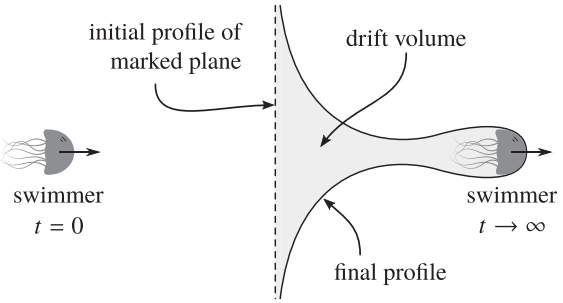

FIG. 1. The drift volume induced by the swimmer is the (shaded) region between the initial and final profiles of a marked plane of fluid.

dioxide, chemicals used for signaling, etc.) that are essential for the survival of the swimmers themselves. For instance, swimmers can increase their rate of feeding by mixing their surroundings as they move [2–4]. Moreover, the possibility that biogenic mixing plays a significant role in the mixing of the oceans has been a subject of intense debate [5–12]. Finally, biomixing is useful from an engineering standpoint. For example, motile bacteria may be used to achieve controlled mixing in microfluidic devices [13,14].

Biomixing induced by swimming microorganisms, such as bacteria, algae, or spermatozoa, has been relatively well characterized. Beginning with the work of Wu and Libchaber [15], several investigators have quantified the diffusion of colloidal particles immersed in a bath of microswimmers using experiments [16–21] and numerical simulations [22–25], or a combination thereof [26–28]. The observed, effective diffusivity of the particles is typically several times greater than their Brownian diffusivity in the absence of swimmers [16]. Drift is central to the theoretical description of this result, since a given colloidal "tracer" particle is advected with the local flow field during an encounter with a swimmer. In the dilute limit, where the volume fraction of swimmers is small, the motion of the tracer may be described by a series of independent hydrodynamic displacements supplied by each swimmer passing close enough to cause appreciable drift. The resulting motion of the tracer is diffusive; the mean-squared displacement thereof grows linearly with time at a rate equal to the *drift diffusivity*. Lin *et al.* [29] computed the tracer trajectories and resulting drift diffusivity in a dilute suspension of micro-swimmers, modeled as "spherical squirmers" that achieve locomotion via steady tangential surface movement [30,31], yielding good agreement with experimental investigations.

Aside from the effective diffusivity due to a suspension of swimmers, quantifying the capacity for an individual swimmer to transport fluid, and hence cause stirring, is also of interest in understanding biogenic mixing. The total amount of fluid transported by a body moving through a fluid via drift is quantified by the *drift volume* [1]. Consider a marked material surface of fluid that initially lies on a flat plane perpendicular to the path of the swimmer. The height of this plane is assumed to be much larger than the size of the swimmer. The drift volume is defined as the total volume of fluid enclosed between the initial and final positions of this material surface as the body translates from far behind to far in front of the initially marked plane (Fig. 1). Leshansky and Pismen [9] and Pushkin *et al.* [32] found that the drift volume due to a steadily translating spherical squirmer in Stokes flow is equal to half of the squirmer's volume. Intriguingly, the same result was obtained by Darwin [1] for a rigid sphere in potential flow. Based on this coincidence, one might expect that the drift diffusivity due to a (noninteracting) suspension of Stokesian squirmers should be comparable to an analogous suspension of translating spheres in potential flow. However, direct comparison of these two scenarios by Lin *et al.* [29] showed that the drift diffusivity induced by the squirmers is instead much larger than the potential flow result [33].

Why do the drift volume and drift diffusivity apparently disagree regarding the extent of swimmer-induced drift? The nature of the flow generated by the swimmer, along with differing assumptions

about the path it traverses, are the cause. In terms of a multipole expansion, the far-field flow around a steadily translating microswimmer that is free from external forces and torques (i.e., a neutrally buoyant swimmer) is dominated by the stresslet (symmetric force dipole) component [34]. The fluid velocity due to the stresslet decays as $1/r^2$, where r is the distance from the swimmer, which is slower than the $1/r^3$ far-field decay associated with potential flow. Thus, the drift diffusivity due to a suspension of Stokesian swimmers is larger than that of an otherwise equivalent suspension of swimmers in potential flow because the overall flow disturbance is longer-ranged in the former case. However, the flow generated by the stresslet is fore-aft mirror symmetric about the plane intersecting the swimmer and normal to its path of motion. Thus, any swimmer traversing a nearly symmetric path, whose start and end points are about equidistant from a tracer particle, will cause the tracer to move along a closed loop with almost zero net displacement [23,29]. The only exceptions are tracers encountering the swimmer nearly head-on, where higher-order flow singularities can impact the tracer's motion. In computing the *total* drift volume, the swimmer's path is always symmetric, starting infinitely far behind and ending infinitely far in front of the marked sheet of fluid tracers. In contrast, the drift diffusivities referred to above are computed under the assumption that each swimmer traverses a finite path before stopping, changing direction randomly, and starting along a new path. These paths are assumed to be randomly distributed, with most of them being asymmetric with respect to the tracer. If the paths traversed by the swimmers were instead infinite, the resulting drift diffusivity would be much smaller because the vast majority of tracers perform closed loops after every encounter with a swimmer. Hence, that the swimmers move a finite distance before changing direction (e.g., the run-and-tumble motion of *E. coli*) is key to the generation of a significant drift diffusivity and subsequent biomixing [29,35].

It is therefore relevant to consider the *partial* drift volume due to the swimmer, or the volume entrained by the swimmer as it travels a finite distance [36,37]. As we will show, while the total drift volume of a solitary Stokesian swimmer in an unbounded fluid is comparable to the volume of the swimmer itself, the partial drift volume is large compared to the swimmer's volume for any path that is asymmetric with respect to the initially marked plane of fluid. In particular, the partial drift volume diverges linearly as the height of the marked plane is made large. A Stokesian swimmer is therefore capable of transporting fluid at scales larger than that of the swimmer itself, reconciling the apparent discrepancy between the drift volume and drift diffusivity as measures of drift-induced transport enhancement.

The drift and subsequent biomixing due to organisms of larger than microscopic size is also of interest, although they have not been as well characterized as they have in Stokes flow. Analysis of the drift due to (Stokesian) microswimmers is simplified because they live in a regime where the ratio of inertial to viscous forces in the fluid is very small. If the density of the fluid is given by ρ and the viscosity by μ, this ratio is given by the Reynolds number, $\mathrm{Re} = \rho U a/\mu$, where U and a are the characteristic speed and length of the body, respectively. For a microswimmer such as a bacterium, which is typically a few microns in size, Re is generally not larger than 10^{-4} in water, and thus results based on Stokes flow ($\mathrm{Re} = 0$) are reliable. However, fluid inertia becomes appreciable for most swimmers larger than about 0.1 mm in size. Furthermore, swimming organisms of sizes between one millimeter to a few centimeters, which typically live at intermediate Reynolds numbers in the range $1 \leqslant \mathrm{Re} \leqslant 1000$, such as small crustaceans, are ecologically important. Due to their large biomass and migratory behaviors, these swimmers have been hypothesized to be a source of potentially important biomixing in lakes and oceans [5], with drift being the primary mechanism through which mixing is accomplished [6]. Therefore, it is important to quantify the drift volume induced by these finite-Re swimmers.

The nonlinearity of the Navier-Stokes equations, which governs the flow, makes analyzing the drift generated by finite-Re swimmers more difficult. Fortunately, some simplification is possible because, at the large scales most relevant to drift, the Navier-Stokes equations may be linearized by using Oseen's approximation. Subramanian [10] and Leshansky and Pismen [9] used this approach to estimate the drift volume due to an idealized swimmer that is assumed to generate a completely steady flow. Under this assumption, the flow sufficiently far from the swimmer is approximately that of the

force-dipole solution to Oseen's equations. It is argued that the total drift volume induced in this case is on the order of that of the swimmer's body and therefore relatively small. This result contrasts with a steady, passively towed body, whose drift volume grows unbounded with time at a rate proportional to the (steady) force applied to the body [36,38]. Critically, the towed body acts as a directed source of momentum in the fluid, which is reflected by a net momentum (and mass) flux through its wake. The thrust and drag components of the force on a steady swimmer are instantaneously balanced (neglecting buoyancy), which leads to a wake with zero mass and momentum fluxes.

However, there are two important aspects of the drift due to finite-Re swimmers that warrant further investigation because they potentially lead to significant large-scale fluid motion. The first one, pointed out by Subramanian [10], concerns the wake of the ideal steady swimmer. Although the wake produces zero net drift volume because of the lack of a net momentum flux, there is still fluid exchange within the wake itself. Specifically, there are separate "thrust" and "drag" contributions to the wake, which contain mass fluxes that are opposite in direction but equal in magnitude. We demonstrate here that both the partial drift volume and the volume of fluid disturbed in the wake are essentially $O(V_b b/\rho U^2 a^3)$, where b is the force dipole observed far from the swimmer and V_b is the volume of the swimmer. Second, the idealization of a completely steady swimmer may be inappropriate because most real swimmers propel themselves unsteadily, periodically changing shape over a stroke cycle (e.g., via moving swimming appendages). The swimmer accelerates during the propulsive phase of the stroke cycle and decelerates during the recovery phase. If we assume that the swimmer does not have a net acceleration over a stroke cycle, then the hydrodynamic force on the swimmer averages to zero. However, due to the nonlinear nature of convective inertia, it is unclear whether the cycle-averaged mass flux through the wake is also zero, as it is for a steady swimmer [9]. Here, we use an integral momentum balance to show definitively that the wake of such an unsteady swimmer *does not* carry a time-averaged net mass flux at sufficiently far distances from the swimmer. Therefore, our results for the drift volume of a steady swimmer at finite Re apply, in a time-averaged sense, to a periodic unsteady swimmer also.

The remainder of this article is structured as follows. In Sec. II, we compute the partial drift volume due to a steady Stokesian swimmer, which is shown to be large compared to the swimmer's volume. This result is due to the long-range flows generated by viscous forces that dominate the entire fluid domain. In Sec. III, we similarly consider the partial drift volume due to a steady swimmer at finite Re. Here, our results suggest that the magnitude of D is highly dependent on the swimming kinematics; it is large compared to V_b only if the swimmer generates a large force dipole. In Sec. IV we consider the time-averaged drift volume due to an unsteady inertial swimmer and show that our steady model remains valid in a time-averaged sense. Also, we show that our simple far-field model is consistent with experiments and direct numerical simulations of real swimmers. Finally, a summary of our findings is offered in Sec. V.

II. A STEADY STOKESIAN SWIMMER

Consider a solitary swimmer of characteristic length a translating with speed U through an unbounded, incompressible Newtonian fluid at $\mathrm{Re} = 0$. For simplicity, we assume that the swimming gait is steady so that neither the swimming velocity nor the fluid velocity (in the comoving frame) are functions of time. We normalize length by a, velocity by U, time t by a/U, and force by $\mu a U$. All quantities defined hereafter are dimensionless unless otherwise stated. Let $\boldsymbol{r} = x\boldsymbol{e}_x + y\boldsymbol{e}_y$ be the position vector relative to the center of the swimmer, where $\boldsymbol{e}_x$ and $\boldsymbol{e}_y$ are the respective axial (x direction) and radial (y direction) unit vectors of a cylindrical coordinate system. Also, let $\boldsymbol{v}(\boldsymbol{r}) = \boldsymbol{u}(\boldsymbol{r}) + \boldsymbol{e}_x$, where $\boldsymbol{u}$ is the fluid velocity in the comoving frame and $\boldsymbol{v}$ is the velocity disturbance (i.e., the instantaneous fluid velocity in the laboratory frame), such that $\boldsymbol{u} = -\boldsymbol{e}_x$ and $\boldsymbol{v} = \boldsymbol{0}$ as $|\boldsymbol{r}| = r \to \infty$. We further assume that the swimmer generates a flow that is axisymmetric about the x axis and free of azimuthal rotation. Therefore, we may define a stream function for $\boldsymbol{u}$ as $\psi_{\boldsymbol{u}}(x,y) = \int y\boldsymbol{u} \cdot (\boldsymbol{e}_x dy - \boldsymbol{e}_y dx)$, with $\psi_{\boldsymbol{u}}(x,0) = 0$. Similarly, we define a (disturbance) stream function for $\boldsymbol{v}$ as $\psi_{\boldsymbol{v}}(x,y) = \psi_{\boldsymbol{u}}(x,y) + y^2/2$.

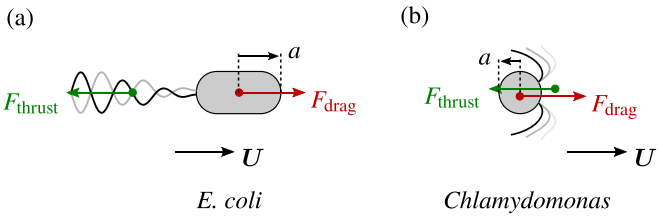

FIG. 2. Pusher (a) and puller (b) type swimmers translate at velocity $\boldsymbol{U}$. Pullers ($b < 0$) are propelled from the front, and hence the center of thrust is in front of the center of drag. Pushers ($b > 0$) are propelled from the rear, where the opposite is true. Note that F_{thrust} and F_{drag}, which are equal and opposite, represent the force exerted by the swimmer on the fluid, and hence F_{thrust} is shown to be directed opposite to the swimming direction.

The fluid flow is governed by the Stokes equations. These equations are linear, and hence the flow may be expressed in terms of a multipole expansion. The leading order term of this expansion is the Stokeslet (force monopole), which yields a velocity decay like $1/r$. The associated stream function is [39, p. 240]

$$\psi_{\boldsymbol{v}}^{(1)} = \frac{y^2}{8\pi r}. \tag{1}$$

However, this term vanishes because there is no net hydrodynamic force on the steadily propelled swimmer [40]; the thrust and drag forces that act on the swimmer are equal in magnitude and opposite in direction. These forces are instead associated with next term in the expansion: the stresslet, i.e., symmetric force dipole. There is no rotlet (antisymmetric force dipole) term because we have assumed axisymmetry about the axis of travel. The stream function corresponding to the stresslet is $\psi_{\boldsymbol{v}}^{(2)} = -\partial\psi_{\boldsymbol{v}}^{(1)}/\partial x$, which corresponds to a velocity field that decays as $1/r^2$. Higher order terms decay more quickly with r. For example, the quadrupolar terms at one order beyond the stresslet are associated with a $1/r^3$ velocity decay. These higher order terms contribute to a more faithful description of the details of the flow near the swimmer, but make a relatively small contribution to the fluid motion at large distances. Thus, we expect their contribution to the drift volume to be small compared to the lowest order stresslet term, and we thus neglect them. We therefore adopt as a model a dipolar point swimmer that produces only a stresslet. The flow produced by this model swimmer is given by

$$\psi_{\boldsymbol{v}} = b\psi_{\boldsymbol{v}}^{(2)} = -b\frac{\partial\psi_{\boldsymbol{v}}^{(1)}}{\partial x}, \tag{2}$$

where b is the strength of the stresslet, which is the magnitude of the thrust and drag forces acting on the swimmer multiplied by their distance of separation.

Depending on the sign of b, a swimmer may fall into one of two categories. If $b < 0$, the swimmer is a "puller," whose center of thrust is in front of its center of drag, and if $b > 0$ the swimmer is a "pusher," whose center of thrust is behind its center of drag (Fig. 2). Microorganisms such as the bacteria *E. coli*, which use flagella to push themselves through their surrounding fluid, exemplify pusher-type swimmers. An example of a puller is given by *Chlamydomonas*, which possesses two flagella that perform a "breast stroke," pulling the organism along. The centers of thrust and drag on the swimmer lie on and are aligned with the x axis due to our assumption of axisymmetric flow.

To compute the swimmer's (partial) drift volume, we consider a material sheet of fluid that is marked (as in with dye) at $t = 0$ and at a distance x_i from the swimmer. Initially, the sheet is a flat, circular disk perpendicular to the x axis and centered on the point $\boldsymbol{r} = x_i\boldsymbol{e}_x$. The partial drift volume D is defined as the volume between the initial and final profiles of this marked material surface and enclosed by the streamtube $\psi_{\boldsymbol{u}} = -h^2/2$ that intersects the outer edge of the marked fluid [36,38]. This streamtube is one of the fluid velocity in the co-moving frame and has radius h as

$x \to \pm\infty$. Moreover, it constitutes a material surface, as does the marked fluid. We may therefore (via mass balance) reinterpret D as the time-integrated volumetric flux through the plane $x = x_i - t$, i.e., the plane (in the laboratory frame) where the fluid is initially marked, and within the streamtube $\psi_{\boldsymbol{u}} = -h^2/2$. Letting $y = y_*(t)$ be the intersection of this plane with the streamtube, the drift volume (normalized by a^3) at $t = t_f$ is then

$$D = \int_0^{t_f} \psi_*(t; x_i, h)dt - [V_b(t_f) - V_b(0)], \tag{3}$$

where $\psi_*(t) = \psi_{\boldsymbol{v}}(x_i - t, y_*(t))$ and $V_b(t)$ is the volume of the swimmer that has passed through $x = x_i - t$. Chisholm and Khair [38] give a detailed derivation of (3).

We are interested in the possibility that the swimmer induces a drift volume that is large compared to its own volume. Thus, we limit our attention to the scenario where the extent of the marked fluid is much larger than that of the swimmer ($h \gg 1$), and where the swimmer moves over a distance that is large compared to its size ($t \gg 1$). In this case, the deviation of the streamtube $\psi_{\boldsymbol{u}} = -h^2/2$ from its free-stream position at $y = h$ is small. Thus, to a leading order approximation in h, we may make the simplification $\psi_*(t) = \psi_{\boldsymbol{v}}(x_i - t, h)$. Let $\tau = (t - x_i)/h$ be the x position of the swimmer, relative to the initially marked plane, normalized by h. Then, $\psi_*(\tau) = \psi_{\boldsymbol{v}}(-h\tau, h)$, and, from (2),

$$\psi_*(\tau) = -b \left.\frac{\partial \psi_{\boldsymbol{v}}^{(1)}}{\partial x}\right|_{(\hat{x},\hat{y})=(-h\tau,h)} = \frac{b}{h}\frac{d\psi_*^{(1)}}{d\tau}. \tag{4}$$

From (4), (3) reduces to

$$D = 2\pi h \int_{\tau_i}^{\tau_f} \psi_*(\tau)d\tau = 2\pi b(\psi_*^{(1)}(\tau_f) - \psi_*^{(1)}(\tau_i)), \tag{5}$$

where $\tau_i = \tau|_{t=0} = -x_i/h$ and $\tau_f = \tau|_{t=t_f} = (t_f - x_i)/h$. The bracketed term in Eq. (3) has been omitted because, in considering a point swimmer, we ignore any effects due to the swimmer occupying a physical volume. From (1),

$$\psi_*^{(1)}(\tau) = \frac{h}{8\pi\sqrt{\tau^2 + 1}}, \tag{6}$$

and, by inserting (6) into (5), we obtain

$$D = \frac{bh}{4}\left(\frac{1}{\sqrt{\tau_f^2 + 1}} - \frac{1}{\sqrt{\tau_i^2 + 1}}\right). \tag{7}$$

as the drift volume due to our model Stokesian swimmer.

Recall that we have taken h to be arbitrarily large, and thus (7) diverges as $h \to \infty$. The cause is the slow $1/r^2$ decay of the velocity disturbance. A similar result is obtained for a towed body, where D diverges as h^2 due to the even slower $1/r$ decay in this case. However, it is reasonable to interpret h as the length scale at which the flow disturbance due to the swimmer is cut off by factors such as the presence of boundaries or other flows not due to the individual swimmer. Thus, as long as this length scale is large, D may be many times larger than the volume of the swimmer itself, indicating that an individual Stokesian swimmer is capable of displacing a relatively large fluid volume as it moves.

From (7), we see that D vanishes in the special case where $\tau_i = -\tau_f$. This particular result reflects the closed-loop paths followed by the marked fluid elements that occur when the swimmer translates symmetrically with respect to the initially marked plane (at $x = x_i$), starting and ending at equal distances behind and ahead of this plane, respectively. These closed-loop paths are a result of the fore-aft mirror symmetry of the velocity field of the stresslet generated by the swimmer. On the other hand, the magnitude of D is maximized when the path traveled by the swimmer is

maximally asymmetric with respect to the marked plane. This corresponds to the scenario where the swimmer starts much nearer to the plane where the fluid is initially marked ($\tau_i \ll 1$) than where it stops and/or changes direction ($\tau_f \gg 1$), or vice versa. Letting $\tau_i \to 0$ and $\tau_f \gg 1$ in Eq. (7) yields $D_{\max} \sim bh/4 \gg 1$. The same result (with the opposite sign of D) is obtained if $-\tau_i \gg 1$ and $\tau_f \ll 1$. Note that D may be positive or negative depending on the sign of b and the values chosen for τ_f and τ_i. A negative D indicates that the majority of the marked fluid has drifted in the negative (rather than positive) x direction.

Experimental measurements [41] and numerical predictions [42] of the flow produced by swimming *E. coli* allow us to estimate $D_{\max}$. From this data, the dipole force is $F_d \approx 1$ pN and the dipole length is $l_d \approx a \approx 2$ μm (comparable to the size of the body of the bacterium), while the swimming velocity is $U \approx 20$ μm/s. Assuming that the bacterium is suspended in water ($\mu \approx 10^{-3}$ Pa s), the (dimensionless) dipole strength is $b = F_d l_d/\mu U a^2 \approx 25$. Hence, we obtain $D_{\max} \approx 6.25h$. In the case that the bacterium is one of many in a dilute suspension, we may roughly estimate h as the average distance between swimmers. If the volume fraction of swimmers is ϕ, then $h \sim \phi^{-1/3}$. Setting $\phi = 0.001$ (as used in the experiments by Jepson *et al.* [20]), we obtain $h \approx 10$, and $D_{\max} \approx 60$. Therefore, the single bacterium transports a volume of fluid that is many times larger than its own via drift. This result suggests that the significant mixing enhancement observed in dilute suspensions of bacteria may be attributed to the large partial drift volume induced by each swimmer as it moves.

Error in the drift volume predicted by (7) comes from two sources. First, we have neglected the contribution of the volume occupied by the swimmer [the bracketed term in Eq. (3)]. The magnitude of this error is $O(1)$, since we have scaled the drift volume by a^3. The second source is from our assumption that the swimmer generates only a stresslet. The quadrupolar (and higher order) components of the fluid velocity, which are only relevant to the near-field flow details, contribute an $O(1)$ amount to D [9,32]. Thus, they are only of significance when the swimmer traverses a symmetric path, for which the contribution from the stresslet vanishes. For any asymmetric path, the partial drift volume is $O(bh)$ due to the stresslet, and thus the error associated with the two aforementioned sources is comparatively small.

In using an idealized, steady model swimmer, we have not explicitly accounted for the effects of a unsteady swimming gait exhibited by virtually all biological swimmers. Doing so is not necessary for a periodic Stokesian swimmer; the linearity of the Stokes equations guarantees that the stroke-cycle-averaged velocity due to the swimmer is also a solution to the (steady) Stokes equations. As a result, steady Stokes flow models faithfully describe the flow produced by microswimmers averaged over many stroke cycles [43]. We expect (7) applies to unsteady swimmers in a time-averaged sense on this basis.

III. A STEADY SWIMMER AT FINITE REYNOLDS NUMBER

We now consider the drift volume due to a swimmer at finite Re. First, we restrict ourselves to a steady swimmer, similar to our preceding analysis of a Stokesian swimmer in Sec. II. If we assume that Re is small but nonzero, we may avoid solving the full Navier-Stokes equations by using Oseen's approximation to the flow. Oseen's equations are linear in the fluid velocity (or the corresponding stream function), and we may express the flow disturbance due to the swimmer in terms of the point-force solution to these equations (the Oseenlet), which is given by the stream function [39, p. 241]

$$\psi_v^{(1)} = \frac{1}{2\pi \mathrm{Re}}\left(1 - \frac{x}{r}\right)\left\{1 - \exp\left[-\frac{\mathrm{Re}}{4}(r + x)\right]\right\}. \tag{8}$$

However, there is no point-force (Oseenlet) component to the flow (which corresponds to the Stokeslet at Re $= 0$) because the swimmer is self-propelled and assumed to be force free. Therefore, the flow due to the swimmer is dominated by the Oseen force dipole (corresponding to the stresslet at Re $= 0$),

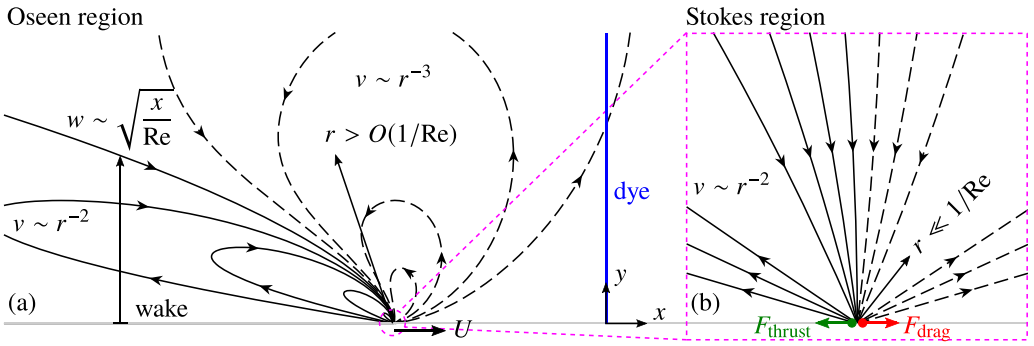

FIG. 3. The lines correspond to streamlines of the far-field flow disturbance (in the laboratory frame), generated by a steady, pusher-type ($b > 0$) swimmer translating at unit speed ($U = 1$) in the $\boldsymbol{e}_x$ direction at $\mathrm{Re} \ll 1$. Arrows indicate the flow direction. Dashed lines indicate positive isocontours of $\psi_{\boldsymbol{v}}$, while solid lines indicate negative isocontours. (a) The flow pattern at distances $r > O(1/\mathrm{Re})$ from the swimmer, in the Oseen region, is affected appreciably by inertia. The initial position of the dyed sheet of fluid is illustrated to the right of the swimmer. A viscous wake of height w grows parabolically with distance downstream of the swimmer. (b) At distances $r \ll 1/\mathrm{Re}$, in the Stokes region, inertial effects are relatively weak and the flow pattern approaches the $\mathrm{Re} = 0$ stresslet. Equivalent plots for a puller ($b < 0$) may be visualized from the above illustration by reversing the streamline directions and the sign of $\psi_{\boldsymbol{v}}$ (but not the swimming direction).

viz.,

$$\psi_{\boldsymbol{v}} = -b\frac{\partial \psi_{\boldsymbol{v}}^{(1)}}{\partial x}, \tag{9}$$

where b is the effective force dipole strength observed at the Oseen level. Due to the nonlinear nature of the Navier-Stokes equations, b is not necessarily the actual force dipole exerted by the swimmer, although the two quantities converge as $\mathrm{Re} \to 0$ [44].

The flow given by (9) is illustrated in Fig. 3. For $h \gg 1$, we may approximate $\psi_*(\tau) = \psi_{\boldsymbol{v}}(-h\tau, h)$ and use (4) in Eq. (5) to give

$$D = \frac{b}{\mathrm{Re}}\left[\left(\frac{\tau}{\sqrt{\tau^2+1}} + 1\right)\left\{1 - \exp\left[-\frac{\mathrm{Re}_h}{4}(-\tau + \sqrt{\tau^2+1})\right]\right\}\right]_{\tau_i}^{\tau_f}, \tag{10}$$

where $[f(\tau)]_{\tau_i}^{\tau_f} \equiv f(\tau_f) - f(\tau_i)$. Here, $\mathrm{Re}_h = \mathrm{Re}h$ is the Reynolds number based on the radius of the initially marked fluid disk. The value of Re_h quantifies how strongly fluid inertia affects the overall motion of the marked fluid elements and therefore the effect of inertia on D. Indeed, Re_h may be interpreted as the ratio of the height of the marked plane h to the Oseen length, $1/\mathrm{Re}$, at which fluid inertia becomes appreciable [38]. The impact of inertia on the flow is significant at distances of $r \geqslant O(1/\mathrm{Re})$ from the swimmer, in the "Oseen region," whereas the impact is small for $r \ll 1/\mathrm{Re}$, in the "Stokes region," where the flow reduces to the (Stokesian) stresslet (Fig. 3). Figure 4 shows the drift volume of the swimmer as a function of Re_h. In order to obtain a universal curve for each value of Re_h, we plot D/bh on the vertical axis. Values of D may be obtained from Fig. 4 for arbitrary τ_f and τ_i by taking the difference of the respective values of D/bh on a given Re_h curve.

Increasing Re (for a fixed value of $h \gg 1$) has two effects. First, D decreases because inertial forces cut off the velocity disturbance created by the swimmer at distances beyond the Oseen length, which may be interpreted as an inertial screening length. The stresslet-like flow in the viscously dominated Stokes region decays as $|\boldsymbol{v}| = v \sim 1/r^2$, whereas the majority of the flow in the inertial Oseen region decays as $v \sim 1/r^3$ (Fig. 3). We see that the expression multiplied by b/Re in Eq. (10) is at most $O(1)$ for all values of τ. Hence, $D = O(b/\mathrm{Re})$. Importantly, the drift volume does not diverge with time for large travel times ($\tau_f \to \infty$), in contrast to a towed body. In the Stokes limit ($\mathrm{Re} \to 0$), the Oseen length diverges, and hence the drift volume is never cut off by inertia. In fact,

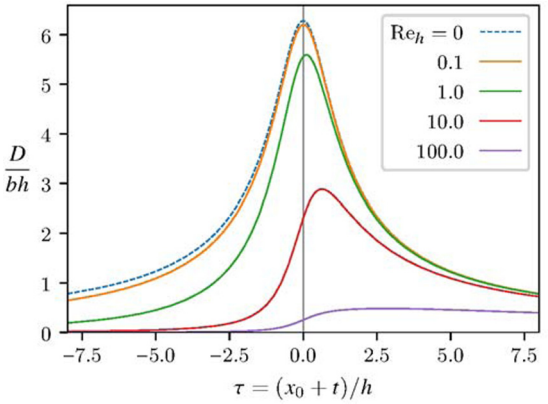

FIG. 4. The (partial) drift volume D is normalized by bh and plotted versus τ. Here, we have taken $\tau_i \to -\infty$ (and $\tau = \tau_f$). The dashed line represents $\mathrm{Re}_h = 0$ (fluid inertia is completely neglected), while the solid lines represent $\mathrm{Re}_h = \{0.1, 1, 10, 100\}$ as the curves respectively descend. The drift volume for arbitrary values of τ_i and τ_f may be obtained by subtracting $D(\tau_i)/bh$ from $D(\tau_f)/bh$ on a chosen Re_h curve.

that (10) diverges as $\mathrm{Re} \to 0$ reflects the divergence of the Stokes-flow result (7) as $h \to \infty$. The second effect of increasing Re is to break the fore-aft symmetry of the flow. As a result, the drift volume does not vanish for a symmetric path ($\tau_f = -\tau_i$), as it does in Stokes flow.

These results are also relevant to swimmers at $\mathrm{Re} \geqslant O(1)$ *if* the flow sufficiently far from the swimmer, which we continue to assume is steady, makes the dominant contribution to D. Here, the far-field flow approximately satisfies Oseen's equations because the disturbance from the free stream is small [45]. However, if the far-field contribution to D is not greater than $O(1)$, then we must also consider the higher-order, near-field contributions to D, which we also expect to be $O(1)$. Most critically, the far-field contribution to D predicted by (10) is $O(b/\mathrm{Re})$. As we shall see in Sec. IV, the magnitude of b/Re depends largely on the details of the particular swimmer of interest. If $b/\mathrm{Re} \gg 1$, then the far-field flow makes the dominant contribution to D, and moreover, D is large compared to the volume of the swimmer. For $\mathrm{Re} \ll 1$, we expect this to generally be the case unless $b \ll 1$. However, if $b/\mathrm{Re} \leqslant O(1)$, then the far-field contribution to D, which is dominant for $\mathrm{Re} \ll 1$, is at most comparable to the $O(1)$ contribution of the near-field flow. Thus, a swimmer at $\mathrm{Re} \geqslant O(1)$ must generate a strong force dipole to induce a large drift volume.

To complete our analysis of the fluid transport due to a steady, finite-Re swimmer, we examine more closely the wake, which accounts for strongest flow disturbance, where $v \sim 1/r^2$ (Fig. 3). The wake is parabolic in shape and is due to viscous forces; vorticity generated by the swimmer is advected downstream and diffuses laterally, while the flow elsewhere remains irrotational and approaches a potential dipole ($v \sim 1/r^3$). The width of the wake is proportional to $1/\mathrm{Re}$, and it diverges at $\mathrm{Re} = 0$, where $v \sim 1/r^2$ everywhere. The *net* flux through the wake of a steady swimmer is zero due to the lack of a net hydrodynamic force. (In contrast, the wake behind a towed body carries a net volumetric flux that is proportional to the drag on the body, resulting in a drift volume that diverges linearly with time [38].) However, the flow is bidirectional [Fig. 3(a)], and the wake contains separate fluxes due to the drag and thrust forces on the swimmer that are equal in magnitude but opposite in direction [10]. This exchange of fluid in the wake is not accounted for by (10); the positive contribution of the drag force effectively cancels with the negative contribution of the thrust.

The flow in the wake sufficiently far downstream of a towed body is obtained by applying a boundary layer analysis to this region (where the body is effectively a point source of momentum) [39, p. 349], yielding

$$\psi_{\boldsymbol{v}}^{(1)} = \frac{1}{\pi \mathrm{Re}} \left(1 - \exp\left[\frac{\mathrm{Re}\, y^2}{8x} \right] \right), \tag{11}$$

for the flow disturbance, which also follows from Taylor expansion of the argument of the exponential in Eq. (8) for small $y/(-x)$. It follows that the flow disturbance in the wake due to a steady, force-free swimmer having the effective force-dipole strength b is given by

$$\psi_{\boldsymbol{v}} = -b\frac{\partial \psi_{\boldsymbol{v}}^{(1)}}{\partial x} = -\frac{by^2}{8\pi x^2}\exp\left(\frac{\mathrm{Re}y^2}{8x}\right). \tag{12}$$

From (12), the x component of the velocity disturbance is

$$v_x = \frac{1}{y}\frac{\partial \psi_{\boldsymbol{v}}}{\partial y} = -\frac{b(\mathrm{Re}y^2+8x)}{x^3}\exp\left(\frac{\mathrm{Re}y^2}{8x}\right). \tag{13}$$

Equation 13 shows that v_x vanishes along the parabolic curve $\mathrm{Re}y^2 + 8x = 0$. If we assume that the swimmer is a pusher ($b > 0$), the wake therefore contains a backward flux ($v_x < 0$) through $y^2 < -8x/\mathrm{Re}$ and a forward flux ($v_x > 0$) through $y^2 > -8x/\mathrm{Re}$. These fluxes are associated with the thrust and drag forces on the swimmer, respectively. The backward part of the flux through the plane $x = x'$ may be obtained from (12) as

$$Q_-(x') = 2\pi\psi_{\boldsymbol{v}}(x', y') = -\frac{2b}{e\mathrm{Re}}\frac{1}{x'}, \tag{14}$$

where $y' = \sqrt{-8x'/\mathrm{Re}}$ is the location at which $v_x = 0$. Note that (14) is only valid for large negative x' where our far-field description of the wake is valid (indeed, Q_- spuriously diverges for small x'). It is easily verified from (12) or (13) that the total flux through any plane $x = x'$ in the wake vanishes. Therefore, the compensating forward flux through the wake is $Q_+ = -Q_- = Q_\pm$.

From (14), the drift volume associated with the opposing fluid fluxes in the wake is

$$D_\pm = \int Q_\pm(x_i - t)dt \sim \frac{2b}{e\mathrm{Re}}\ln t. \tag{15}$$

Thus, the amount of fluid exchanged in the wake diverges as $t \to \infty$. However, this divergence is logarithmic (i.e., weak), and $\ln t$ does not grow very large even if the swimmer travels for a reasonably long time. At very long travel times, background flows or density stratification in the fluid would be expected to cut off the wake fluxes anyway. Thus, for a large volume of fluid to be exchanged in the wake, we require b/Re to be large, which is the same prefactor that appears in Eq. (10).

IV. DRIFT VOLUME INDUCED BY AN UNSTEADY INERTIAL SWIMMER

As stated in Sec. II, estimates of the drift volume due to an idealized steady swimmer at $\mathrm{Re} = 0$ are also applicable to unsteady swimmers in a time-averaged sense due to the linearity of the Stokes equations. The (time-averaged) drift volume due to an unsteady swimmer is therefore the same as that due to a steady swimmer at $\mathrm{Re} = 0$, given that the effective force-dipole strength is the same for both swimmers. The situation is different for unsteady swimmers at nonzero Re. Addressing this case is important because the majority of inertial swimming organisms move in an unsteady fashion over a stroke cycle, notwithstanding the possibility that their swimming velocity averaged over a cycle is relatively constant during locomotion over times long compared to the stroke period. Specifically, a time-averaged unsteady flow field does not, in general, satisfy the steady Navier-Stokes equations due to the nonlinear nature of convective inertia. Thus, even if the net force on an unsteady swimmer is zero over a stroke cycle (i.e., it does not experience a net acceleration), it is unclear whether the net momentum flux through the swimmer's wake is zero. If a nonzero net flux were to exist, then an unsteady finite Re swimmer could generate a drift volume that diverges linearly with travel time, in the same manner as a towed body, as suggested by Leshansky and Pismen [9]. In contrast, if the net flux is zero, then our analysis of a steady inertial swimmer in Sec. III holds and suggests that a smaller, convergent (partial) drift volume is generated, which is $O(V_b b/\mathrm{Re})$.

We may determine information about the flow far from the swimmer, as is most relevant to large scale drift, by applying an integral momentum balance to the fluid around the swimmer. We define a

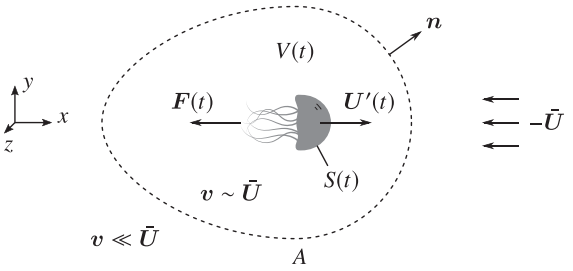

FIG. 5. A control volume $V(t)$ surrounds an unsteady, self-propelled swimmer. The reference frame translates at the constant, time-averaged velocity $\bar{\boldsymbol{U}}$ of the swimmer over a periodic swimming stroke cycle. In this frame, the swimmer periodically fluctuates about a central position at velocity $\boldsymbol{U}'(t)$, and exerts the instantaneous force $\boldsymbol{F}(t)$ on V as it accelerates and decelerates. The outer bounding surface A is fixed and assumed to be far enough from the swimmer such that the fluid velocity beyond A is only disturbed slightly from free stream ($\boldsymbol{v} \ll \bar{\boldsymbol{U}}$). The inner boundary $S(t)$ coincides with the moving surface of the swimmer's body.

control volume $V(t)$ surrounding the swimmer, whose inner boundary $S(t)$ coincides with the moving surface of the swimmer's body, and whose outer boundary A is fixed in the reference frame moving with the stroke-cycle-averaged velocity $\bar{\boldsymbol{U}}$ of the swimmer, as illustrated in Fig. 5. We consider $S(t)$ to be a no-slip boundary, while fluid passes unaffected through A. We denote the stroke-cycle average of an arbitrary function of time $h(t)$ as $\bar{h} \equiv (1/T)\int_{t_0}^{t_0+T} h(t)dt$, where T is the period of the stroke. We assume that the swimmer's motion is periodic so that $\bar{\boldsymbol{U}}$ is a constant. The chosen reference frame is thus inertial. The integral momentum balance on $V(t)$ is then, in terms of dimensional quantities,

$$\frac{d}{dt}\int_{V(t)} \rho \boldsymbol{u} dV - \int_{S(t)} \boldsymbol{\sigma}\cdot\boldsymbol{n} dS + \int_{A} (\rho \boldsymbol{u}\boldsymbol{u} - \boldsymbol{\sigma})\cdot\boldsymbol{n} dA = \boldsymbol{0}, \tag{16}$$

where $\boldsymbol{\sigma}$ is the stress tensor and $\boldsymbol{n}$ is the unit normal vector facing out of V. Gravity does not explicitly appear in Eq. (16) because we have absorbed it into the isotropic part of $\boldsymbol{\sigma}$ (i.e., a modified pressure is used).

The instantaneous hydrodynamic force acting on the swimmer is $\boldsymbol{F}(t) = -\int_{S(t)} \boldsymbol{\sigma}\cdot\boldsymbol{n} dS$ (the minus sign is due to the orientation of $\boldsymbol{n}$), which appears as the second term in Eq. (16). The dependence of $\boldsymbol{F}(t)$ on the swimming velocity $\boldsymbol{U}(t)$ is nontrivial: even in the relatively simple case of unsteady Stokes flow, $\boldsymbol{F}(t)$ contains contributions from the quasisteady Stokes drag; added mass force, or acceleration reaction; and the Bassett, or memory, force [40]. At small Re, this dependence is even more complicated due to the action of convective inertia at the Oseen scale [46]. Fortunately, explicit knowledge of $\boldsymbol{F}(t)$ is not needed; we only insist that $\boldsymbol{F}(t)$ vanishes over a stroke cycle. For a neutrally buoyant swimmer, the hydrodynamic force is the only force acting on the swimmer. Therefore, $\boldsymbol{F}(t) = m\boldsymbol{a}$, where m is the swimmer's mass and $\boldsymbol{a} = \boldsymbol{a}(t)$ is its acceleration. The vector $\boldsymbol{P}(t) = \int_A (\rho\boldsymbol{u}\boldsymbol{u} - \boldsymbol{\sigma})\cdot\boldsymbol{n}$ denotes the rate at which momentum is transferred through A to the fluid lying outside of $V(t)$, which is precisely the integral over A in Eq. (16). Thus, we may rewrite (16) as

$$\frac{d}{dt}\int_{V(t)} \rho \boldsymbol{u} dV + m\boldsymbol{a} + \boldsymbol{P} = \boldsymbol{0}. \tag{17}$$

We select all of A to be sufficiently far from the swimmer such that the fluid velocity there differs only marginally from that of the undisturbed flow. That is, $\boldsymbol{v} \ll \bar{\boldsymbol{U}}$ on A, where $\boldsymbol{v}(t) = \boldsymbol{u}(t) - \bar{\boldsymbol{U}}$ is the velocity disturbance due to the swimmer. At small Re, the required distance of points on A from the swimmer is on the order of the Oseen length a/Re; this distance becomes shorter with increasing Re due to increasing ability of inertia to screen the velocity disturbance caused by the swimmer. At larger Re, this distance will depend the details of the swimming kinematics, but is expected to be within a few body lengths of the swimmer. Then, very far from the swimmer (e.g., distances much

larger than a/Re for small Re), where all of A effectively shrinks to a point, the flow satisfies Oseen's equations forced by a point source of momentum of strength $\boldsymbol{P}(t)$ at the origin, that is,

$$\rho\left(\frac{\partial \boldsymbol{u}}{\partial t} - \bar{\boldsymbol{U}} \cdot \nabla \boldsymbol{u}\right) = -\nabla p + \mu \nabla^2 \boldsymbol{u} + [\boldsymbol{P}(t)\delta(\boldsymbol{r}) + \boldsymbol{B}(t) \cdot \nabla\delta(\boldsymbol{r}) + \cdots], \tag{18}$$

where $\boldsymbol{r}$ is the position vector, $\delta(\boldsymbol{r})$ is the three-dimensional Dirac delta function, and p is the (modified) pressure. We have also included the contribution from the force dipole having the effective (tensorial) strength $\boldsymbol{B}(t)$. We neglect higher-order multipole contributions to the flow (e.g., from the force quadrupole), since these contributions decay more quickly with r, rendering their contribution to the large scale drift small.

If the period T of a swimming stroke cycle is much shorter than the total travel time of the swimmer, then the time dependence of the flow over each stroke cycle is unimportant [10]. Hence, taking the stroke-cycle average of (18) yields

$$-\rho(\bar{\boldsymbol{U}} \cdot \nabla)\bar{\boldsymbol{u}} = -\nabla \bar{p} + \mu \nabla^2 \bar{\boldsymbol{u}} + \bar{\boldsymbol{P}}\delta(\boldsymbol{r}) + \bar{\boldsymbol{B}} \cdot \nabla\delta(\boldsymbol{r}), \tag{19}$$

revealing that the far-field time-averaged flow satisfies the steady Oseen equations, which is expected because these equations are linear in $\boldsymbol{u}$. From (17), the time-averaged momentum source is

$$\bar{\boldsymbol{P}} = -m\bar{\boldsymbol{a}} - \overline{\frac{d}{dt}\int_{V(t)} \rho \boldsymbol{u}\, dV}. \tag{20}$$

The first term on the right-hand side of (20) is zero because we assume that the swimmer does not have a net acceleration over a stroke cycle. The second term represents the rate of change of the fluid momentum in $V(t)$ over a stroke cycle and is equal to $\int_{V(t)} \rho \boldsymbol{u}(\boldsymbol{r}, t+T)dV - \int_{V(t)} \rho \boldsymbol{u}(\boldsymbol{r}, t)dV$. We also expect this term to vanish because momentum cannot continually accumulate in V over each (periodic) stroke cycle. Thus, $\bar{\boldsymbol{P}} = 0$. Consequently, the time-averaged flow far from the swimmer is dominated by the force dipole, implying that the time-averaged net flux through the wake of an unsteady (periodic) swimmer vanishes. Since we assume that the trajectory of the swimmer, on average, is rectilinear, it is reasonable to assume that the mean flow far from the swimmer is axisymmetric with respect to the path of travel. Therefore, the analysis of a steady, finite-Re swimmer in Sec. III applies also to an unsteady, periodic swimmer in a time-averaged sense.

Our model makes three main predictions for the time-averaged, far-field flow of a periodic swimmer: (i) the velocity in the wake decays as $1/r^2$, while elsewhere it approaches a potential dipole ($\boldsymbol{v} \sim 1/r^3$) as the distance from the swimmer becomes large; (ii) the wake of swimmer contains no net mass or momentum flux; and (iii) the drift volume is $O(b/\mathrm{Re})$. Prediction (ii) represents a fundamental difference with the case of an towed body, where the wake contains a momentum surplus equal to the external force on the body. These predictions apply if (i) the instantaneous flow about the swimmer is laminar and axially symmetric about the swimming direction and (ii) there is no net acceleration over a stroke cycle, such that cycle-averaged swimming velocity is constant during locomotion. The latter restriction excludes the case of a swimmer starting from rest (or coming to a stop). Specifically, there would be a net momentum flux during the period of time before a steady average swimming velocity is attained. If that period is comparable to the total travel time of the swimmer, then our predictions above for the drift volume would not be accurate. The assumption of laminar, axisymmetric flow excludes the important case where Re is large enough that the flow becomes fully three-dimensional and possibly turbulent in the near field of the swimmer. Analyzing the drift volume in such instances is clearly a nontrivial task. However, provided one is interested only in large-scale drift, our assumption of laminar flow is acceptable, since turbulent wakes eventually evolve into a laminar state sufficiently far downstream from a swimmer (and also a towed body, for that matter) [10].

Experiments and direct numerical simulations (DNS) of actual swimmers give results that are consistent with the time-averaged, far-field flow structure suggested by our model (Fig. 3). For example, Yeo *et al.* [47] performed DNS of a freely swimming fish at Re of 100 to 5000. These

simulations show that the flow outside of the wake and just beyond the immediate vicinity of the fish's body strongly resembles a potential dipole (a source/sink pair of fluid mass), as we predict. The flow inside the wake takes the form of a reverse Kármán vortex street, a flow structure that is strongly associated with thrust production by undulatory swimmers [48]. The Kármán vortex street consists of a chain of vortex rings of alternating sign and contains no time-averaged mass flux, given that the swimmer has attained a steady average velocity (see Figs. 1 and 7 in Ref. [49]). The lack of a time-averaged, streamwise mass flux in the unsteady wake of a fish is also observed in the DNS performed by Maertens *et al.* [50]. These simulations show that the mean velocity disturbance jets away from the fish along the axis of travel but reverses direction around the edges of the jet to give a wake that is altogether momentumless, similar to what is shown in Fig. 3(a). Furthermore, particle image velocimetry (PIV) measurements of the turbulent wake behind an eel, of about 40 cm in length and swimming at about two body lengths per second, indicate an axial velocity profile that, when averaged over several stroke cycles (with a single cycle corresponding to a tail beat), is also nearly momentumless [51]. Finally, the experiments of Kiorboe *et al.* [52] confirm the predicted $1/r^2$ velocity decay in the wake of a freely swimming *Metridia longa*, a copepod of a few millimeters in length.

It is instructive to estimate D for actual swimming organisms. Recall, in Sec. III, the dimensional drift volume due to a finite-Re swimmer was determined to be $D/V_b = O(b/\mathrm{Re})$, where b is a dimensionless force-dipole strength and V_b is the volume of the swimmer. First, consider a copepod (a small crustacean) of size $a \approx 0.5$ mm swimming at speed $|\bar{\boldsymbol{U}}| = \bar{U} \approx 2$ mm/s in water ($\rho = 1 \times 10^3$ kg/m^3, $\mu = 1 \times 10^{-3}$ Pa s), which corresponds to $\mathrm{Re} \approx 1$. Jiang *et al.* [53] estimated that the thrust produced by such a copepod is approximately 0.1 μN. If we use this value for the dipole force F_d and assume that the dipole length is $l_d \sim a$, then the resulting estimate of the (viscously scaled) force-dipole strength is $b = F_d/\mu\bar{U}a \approx 100$. Therefore, we estimate $D = O(100V_b)$. Next, consider the ascidian larva *Botrylloides* sp., whose locomotion is analyzed in detail by McHenry [54]. This tadpole-like swimmer is about 2 mm in length and swims at approximately 30 mm/s, giving $\mathrm{Re} \approx 60$. It produces thrust and drag forces of approximately 6 μN, which yield $b \sim O(100)$. Then, estimating as before, we obtain $D/V_b \sim b/\mathrm{Re} \sim 1.6$. Last, we consider the jellyfish *Aurelia*, which has a bell radius of approximately 5 cm. Experiments and simulations by McHenry and Jed [55] show that such jellyfish produce approximately 5 mN of thrust and travel at an average speed of 2 cm/s. From these values, $\mathrm{Re} = 1000$ and $b = 2 \times 10^{-4}$, which give $D \sim 20V_b$.

The estimated $O(100V_b)$ drift volume due to the copepod mentioned above is significantly larger than the volume of the copepod itself. In contrast, *Botrylloides* sp., which swims at $\mathrm{Re} \approx 60$, produces an estimated drift volume that is only $O(V_b)$. Both swimmers generate similar dipole strengths of $b \sim 100$. Therefore, we may attribute the reduction in D for the latter swimmer to the larger Re; the stronger inertial screening of viscous forces lessens the flow disturbance and hence inhibits the drift. Interestingly, *Aurelia* swims at an even higher Re of 1000, but produces a very large estimated force dipole strength of $b = 2 \times 10^4$. The drift volume produced by this jellyfish is therefore estimated to be an order of magnitude larger than the volume of the swimmer. Experiments by Katija and Dabiri [6] and Nawroth and Dabiri [56], which use dye to track the drift generated by jellyfish, appear to be in qualitative agreement with this result.

It is helpful to realize that b/Re is just the inertially scaled force-dipole strength of the swimmer (equal to $F_d l_d/\rho U^2 a^3$ in dimensional terms), and D is simply proportional to this quantity. If we assume that the dipole length l_d is on the order of the swimmer's size a, then $b/\mathrm{Re} \sim F_d/\rho\bar{U}^2a^2$, which is analogous to the drag coefficient of a towed body with the dipole force F_d playing the role of the drag force. The drag coefficient of a towed body ranges in magnitude depending on Re and the shape of the particular body in question. Thus, we expect that something similar may be true of the force-dipole strength of a self-propelled swimmer. Comparing *Botrylloides* sp. ($b/\mathrm{Re} \sim 1.6$) to *Aurelia* ($b/\mathrm{Re} \sim 20$), we see their modes of locomotion are quite different. *Botrylloides* swims in a continuous, undulatory fashion, while *Aurelia* uses pulsed jet propulsion (rapid jetting followed by a period of coasting). The swimming style of the latter apparently gives rise to a much stronger effective force dipole than the former, which is perhaps due to the greater *temporal* separation of

thrust and drag. Interestingly, pulsed jet swimmers also have a notably higher cost of transport compared to undulatory swimmers like fish [57]. The cost of transport is a dimensionless measure of self-propulsion efficiency defined as $\mathrm{COT} = P/WU$, where P is power expended by the swimmer, W is the swimmer's weight, and U is the velocity. Our results seem to indicate that, although a jetting swimmer (like a jellyfish) is relatively inefficient in terms of forward propulsion, some of the power it expends creates potentially useful fluid stirring in the form of drift.

V. SUMMARY

We have analyzed the partial drift volume D induced by a self-propelled swimmer in a homogeneous Newtonian fluid. In Stokes flow, D is generally large compared to the volume of the swimmer itself based on our predictions for an idealized steady swimmer that exerts a force dipole on the fluid. The exception to the above statement occurs when a swimmer's path starts and ends at nearly equal distances from the initial position of the marked fluid disk. In that instance, the fore-aft mirror symmetry of the stresslet flow dictates that the partial drift volume is on the order of the swimmer's size. Aside from this special case, D diverges as the height of the marked plane of fluid under consideration (ah) is made large. This implies that the drift volume is only limited by the presence of boundaries or other physical factors (e.g., density stratification) that screen the $1/r^2$ decay of the stresslet velocity disturbance due to the swimmer. Stokesian swimmers are therefore capable of transporting large fluid volumes via partial drift, explaining their effectiveness as biomixers.

We also considered a similar steady swimmer at nonzero Re. Here, D does not diverge as $h \to \infty$ because inertia screens the flow disturbance due to the swimmer. At small Re, this screening occurs at the Oseen length a/Re, where the effect of convective inertia in sweeping vorticity past the swimmer is comparable to vorticity diffusion. Therefore, the $1/r^2$ decay of the stresslet flow in the near field of the swimmer (where vorticity diffusion dominates) eventually transitions to a faster $1/r^3$ decay within the majority of the Oseen region, characteristic of a potential dipole. This flow pattern results in a partial drift volume of $O(V_b b/\mathrm{Re})$, where b is the dimensionless force-dipole strength. This result is consistent with our prediction that $D/V_b = O(bh)$ in Stokes flow; ah is the height of the marked plane, which can be viewed as a length scale at which other physical effects impact the drift. At small Re it is natural to take $h = 1/\mathrm{Re}$, the additional physical effect at this scale being that of inertia, which indeed recovers $D/V_b = O(b/\mathrm{Re})$. The result $D/V_b = O(b/\mathrm{Re})$ holds at $\mathrm{Re} \gtrsim O(1)$ provided that the far-field flow makes the dominant contribution to D. Thus, if the dimensionless dipole strength $b/\mathrm{Re} = O(1)$, then D is comparable to the swimmer's volume, as was exemplified by an estimate of D for *Botrylloides* sp. However, b/Re is not necessarily small when Re is large, as exemplified by *Aurelia*, and its value depends heavily on the kinematics of the swimmer. We also considered the wake of the swimmer, where viscous forces remain relevant and the velocity decays as $1/r^2$. We showed that, although there is no net volume flux through the wake of a steady swimmer, there are equal but opposite volumes of fluid exchanged within the wake that essentially cancel. A detailed consideration of the drift volumes due to these separate fluxes yielded $D_\pm/V_b \sim (b/\mathrm{Re}) \ln t$, which grows only very slowly for long travel times due to the logarithmic time dependence.

Our results for a steady finite Re swimmer also apply, in a time-averaged sense, to an unsteady inertial swimmer that does not experience a net acceleration over a stroke cycle. The key to this conclusion was the demonstration, via an integral momentum balance, that such a swimmer does not act as a net source of momentum over a stroke cycle. Therefore, the large-scale flow is determined by the average force dipole due to the swimmer, which results in an average wake flow that is devoid of a net momentum flux, per our analysis of a steady swimmer. Indeed, this picture of the flow is corroborated by experiments and direct numerical simulations of real swimmers. However, there are important classes of unsteady locomotion that are not covered by our analysis, as mentioned in Sec. IV.

Finally, it is important to emphasize that we have considered a solitary swimmer; therefore, our conclusions are only relevant to suspensions that are sufficiently dilute for interactions between organisms to be negligible. Beyond the dilute limit, interactions between individual swimmers

could profoundly impact the drift in a suspension undergoing a net directed migration [9]. Indeed, experiments on vertically migrating *Artemia salina* (a species of shrimp about 15 mm in length; an intermediate Re swimmer) suggest that hydrodynamic interactions lead to flow structures, and eventual hydrodynamic instabilities, on a scale that is significantly larger than that of an individual organism [58]. An ability to predict the drift due to nondilute suspensions of inertial swimmers is thus of clear interest, but we must defer this interesting topic to future work.

[1] C. Darwin, Note on hydrodynamics, Math. Proc. Cambridge Philos. Soc. **49**, 342 (1953).
[2] V. Magar, T. Goto, and T. J. Pedley, Nutrient uptake by a self-propelled steady squirmer, Q. J. Mechanics Appl. Math. **56**, 65 (2003).
[3] V. Magar and T. J. Pedley, Average nutrient uptake by a self-propelled unsteady squirmer, J. Fluid Mech. **539**, 93 (2005).
[4] S. Michelin and E. Lauga, Optimal feeding is optimal swimming for all Péclet numbers, Phys. Fluids **23**, 101901 (2011).
[5] W. K. Dewar, R. J. Bingham, R. L. Iverson, D. P. Nowacek, L. C. St. Laurent, and P. H. Wiebe, Does the marine biosphere mix the ocean? J. Mar. Res. **64**, 541 (2006).
[6] K. Katija and J. O. Dabiri, A viscosity-enhanced mechanism for biogenic ocean mixing, Nature (London) **460**, 624 (2009).
[7] J. O. Dabiri, Role of vertical migration in biogenic ocean mixing, Geophys. Res. Lett. **37**, L11602 (2010).
[8] A. W. Visser, Biomixing of the oceans? Science **316**, 838 (2007).
[9] A. M. Leshansky and L. M. Pismen, Do small swimmers mix the ocean? Phys. Rev. E **82**, 025301 (2010).
[10] G. Subramanian, Viscosity-enhanced bio-mixing of the oceans, Curr. Sci. **98**, 1103 (2010).
[11] E. Kunze, Fluid mixing by swimming organisms in the low-Reynolds-number limit, J. Mar. Res. **69**, 591 (2011).
[12] K. Katija, Biogenic inputs to ocean mixing, J. Exp. Biol. **215**, 1040 (2012).
[13] M. J. Kim and K. S. Breuer, Enhanced diffusion due to motile bacteria, Phys. Fluids **16**, L78 (2004).
[14] M. J. Kim and K. S. Breuer, Controlled mixing in microfluidic systems using bacterial chemotaxis, Anal. Chem. **79**, 955 (2007).
[15] X.-L. Wu and A. Libchaber, Particle Diffusion in a Quasi-Two-Dimensional Bacterial Bath, Phys. Rev. Lett. **84**, 3017 (2000).
[16] K. C. Leptos, J. S. Guasto, J. P. Gollub, A. I. Pesci, and R. E. Goldstein, Dynamics of Enhanced Tracer Diffusion in Suspensions of Swimming Eukaryotic Microorganisms, Phys. Rev. Lett. **103**, 198103 (2009).
[17] G. Miño, T. E. Mallouk, T. Darnige, M. Hoyos, J. Dauchet, J. Dunstan, R. Soto, Y. Wang, A. Rousselet, and E. Clement, Enhanced Diffusion Due to Active Swimmers at a Solid Surface, Phys. Rev. Lett. **106**, 048102 (2011).
[18] H. Kurtuldu, J. S. Guasto, K. A. Johnson, and J. P. Gollub, Enhancement of biomixing by swimming algal cells in two-dimensional films, Proc. Natl. Acad. Sci. USA **108**, 10391 (2011).
[19] G. L. Miño, J. Dunstan, A. Rousselet, E. Clément, and R. Soto, Induced diffusion of tracers in a bacterial suspension: Theory and experiments, J. Fluid Mech. **729**, 423 (2013).
[20] A. Jepson, V. A. Martinez, J. Schwarz-Linek, A. Morozov, and W. C. K. Poon, Enhanced diffusion of nonswimmers in a three-dimensional bath of motile bacteria, Phys. Rev. E **88**, 041002 (2013).
[21] A. E. Patteson, A. Gopinath, P. K. Purohit, and P. E. Arratia, Particle diffusion in active fluids is non-monotonic in size, Soft Matter **12**, 2365 (2016).
[22] P. T. Underhill, J. P. Hernandez-Ortiz, and M. D. Graham, Diffusion and Spatial Correlations in Suspensions of Swimming Particles, Phys. Rev. Lett. **100**, 248101 (2008).
[23] J. Dunkel, V. B. Putz, I. M. Zaid, and J. M. Yeomans, Swimmer-tracer scattering at low Reynolds number, Soft Matter **6**, 4268 (2010).
[24] T. Ishikawa, J. T. Locsei, and T. J. Pedley, Fluid particle diffusion in a semidilute suspension of model micro-organisms, Phys. Rev. E **82**, 021408 (2010).

[25] A. Morozov and D. Marenduzzo, Enhanced diffusion of tracer particles in dilute bacterial suspensions, Soft Matter **10**, 2748 (2014).
[26] C. Valeriani, M. Li, J. Novosel, J. Arlt, and D. Marenduzzo, Colloids in a bacterial bath: Simulations and experiments, Soft Matter **7**, 5228 (2011).
[27] T. V. Kasyap, D. L. Koch, and M. Wu, Hydrodynamic tracer diffusion in suspensions of swimming bacteria, Phys. Fluids **26**, 081901 (2014).
[28] R. Jeanneret, D. O. Pushkin, V. Kantsler, and M. Polin, Entrainment dominates the interaction of microalgae with micron-sized objects, Nat. Commun. **7**, 12518 (2016).
[29] Z. Lin, J.-L. Thiffeault, and S. Childress, Stirring by squirmers, J. Fluid Mech. **669**, 167 (2011).
[30] M. J. Lighthill, On the squirming motion of nearly spherical deformable bodies through liquids at very small Reynolds numbers, Commun. Pure Appl. Math. **5**, 109 (1952).
[31] J. R. Blake, A spherical envelope approach to ciliary propulsion, J. Fluid Mech. **46**, 199 (1971).
[32] D. O. Pushkin, H. Shum, and J. M. Yeomans, Fluid transport by individual microswimmers, J. Fluid Mech. **726**, 5 (2013).
[33] J.-L. Thiffeault and S. Childress, Stirring by swimming bodies, Phys. Lett. A **374**, 3487 (2010).
[34] E. Lauga and T. R. Powers, The hydrodynamics of swimming microorganisms, Rep. Prog. Phys. **72**, 096601 (2009).
[35] D. O. Pushkin and J. M. Yeomans, Fluid Mixing by Curved Trajectories of Microswimmers, Phys. Rev. Lett. **111**, 188101 (2013).
[36] I. Eames, S. E. Belcher, and J. C. R. Hunt, Drift, partial drift and Darwin's proposition, J. Fluid Mech. **275**, 201 (1994).
[37] R. Camassa, R. M. McLaughlin, M. N. J. Moore, and A. Vaidya, Brachistochrones in potential flow and the connection to Darwin's theorem, Phys. Lett. A **372**, 6742 (2008).
[38] N. G. Chisholm and A. S. Khair, Drift volume in viscous flows, Phys. Rev. Fluids **2**, 064101 (2017).
[39] G. K. Batchelor, *An Introduction to Fluid Mechanics* (Cambridge University Press, Cambridge, 1967).
[40] S. Kim and S. J. Karrila, *Microhydrodynamics: Principles and Selected Applications*, Butterworth-Heinemann Series in Chemical Engineering (Butterworth-Heinemann, Boston, 1991).
[41] K. Drescher, J. Dunkel, L. H. Cisneros, S. Ganguly, and R. E. Goldstein, Fluid dynamics and noise in bacterial cell-cell and cell-surface scattering, Proc. Natl. Acad. Sci. USA **108**, 10940 (2011).
[42] J. Dunstan, G. Miño, E. Clement, and R. Soto, A two-sphere model for bacteria swimming near solid surfaces, Phys. Fluids **24**, 011901 (2012).
[43] K. Drescher, R. E. Goldstein, N. Michel, M. Polin, and I. Tuval, Direct Measurement of the Flow Field around Swimming Microorganisms, Phys. Rev. Lett. **105**, 168101 (2010).
[44] A. S. Khair and N. G. Chisholm, Expansions at small Reynolds numbers for the locomotion of a spherical squirmer, Phys. Fluids **26**, 011902 (2014).
[45] Y. D. Afanasyev, Wakes behind towed and self-propelled bodies: Asymptotic theory, Phys. Fluids **16**, 3235 (2004).
[46] P. M. Lovalenti and J. F. Brady, The hydrodynamic force on a rigid particle undergoing arbitrary time-dependent motion at small Reynolds number, J. Fluid Mech. **256**, 561 (1993).
[47] K. S. Yeo, S. J. Ang, and C. Shu, Simulation of fish swimming and manoeuvring by an SVD-GFD method on a hybrid meshfree-Cartesian grid, Comput. Fluids **39**, 403 (2010).
[48] G. S. Triantafyllou, M. S. Triantafyllou, and M. A. Grosenbaugh, Optimal thrust development in oscillating foils with application to fish propulsion, J. Fluids Struct. **7**, 205 (1993).
[49] C. Eloy, Optimal Strouhal number for swimming animals, J. Fluids Struct. **30**, 205 (2012).
[50] A. P. Maertens, A. Gao, and M. S. Triantafyllou, Optimal undulatory swimming for a single fish-like body and for a pair of interacting swimmers, J. Fluid Mech. **813**, 301 (2017).
[51] E. D. Tytell, Do trout swim better than eels? Challenges for estimating performance based on the wake of self-propelled bodies, Exp. Fluids **43**, 701 (2007).
[52] T. Kiorboe, H. Jiang, R. J. Goncalves, L. T. Nielsen, and N. Wadhwa, Flow disturbances generated by feeding and swimming zooplankton, Proc. Natl. Acad. Sci. USA **111**, 11738 (2014).
[53] H. Jiang, T. R. Osborn, and C. Meneveau, The flow field around a freely swimming copepod in steady motion. Part I: Theoretical analysis, J. Plankton Res. **24**, 167 (2002).

[54] M. J. McHenry, The hydrodynamics of locomotion at intermediate Reynolds numbers: Undulatory swimming in ascidian larvae (Botrylloides sp.), J. Exp. Biol. **206**, 327 (2003).
[55] M. J. McHenry and J. Jed, The ontogenetic scaling of hydrodynamics and swimming performance in jellyfish (Aurelia aurita), J. Exp. Biol. **206**, 4125 (2003).
[56] J. C. Nawroth and J. O. Dabiri, Induced drift by a self-propelled swimmer at intermediate Reynolds numbers, Phys. Fluids **26**, 091108 (2014).
[57] R. N. Govardhan and J. H. Arakeri, Fluid mechanics of aquatic locomotion at large Reynolds numbers, J. Indian Inst. Sci. **91**, 429 (2011).
[58] M. M. Wilhelmus and J. O. Dabiri, Observations of large-scale fluid transport by laser-guided plankton aggregations, Phys. Fluids **26**, 101302 (2014).